JOURNAL OF SOLID STATE CHEMISTRY 56, 211–224 (1985)

Some Aspects of the Dependence of Solid-State Structure on Electron Count

JEREMY K. BURDETT[1] AND STEPHEN LEE

Chemistry Department, The University of Chicago, Chicago, Illinois 60637

Received May 25, 1984

The method of moments is used to show how the structures of molecules and solids is sensitive to the number of valence electrons.

Introduction

The property of a molecule or solid which enables determination of the electronic energy of the system is the energy density of states $\rho(e)$ shown in **1** and **2**. In

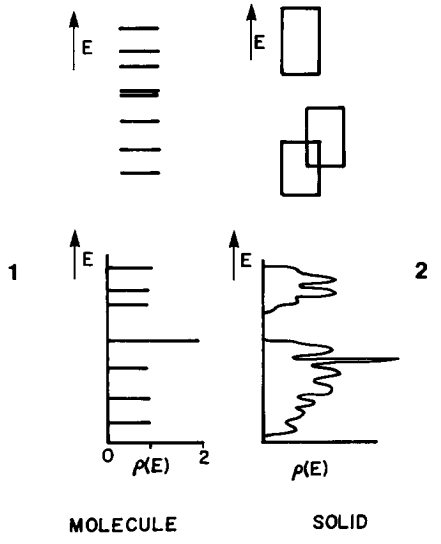

the molecular case the energy spectrum is discrete but in the solid state the atomic levels are broadened into energy bands and the spectrum is a continuous one. The one-electron energy of the molecule or solid is simply given by

$$\text{molecule} \qquad E = 2\sum_{i=i}^{h} \rho(e)e_i \qquad (1)$$

$$\text{solid} \qquad E = 2\int_{-\infty}^{e_F} \rho(e)e \cdot de, \qquad (2)$$

where e_F is the Fermi energy, the energy of the highest occupied level in the solid, corresponding to the HOMO (level h) of the molecule. Theoretical effort in determining the energy of a molecular- or solid-state system is directed toward calculation $\rho(e)$. In the solid state the location of e_F is particularly important in controlling many of the transport properties of such materials. For example, a high density of states at the Fermi level appears to be crucial for high T_c superconductors. Calculations which are good enough to locate the Fermi level at a narrow spike in $\rho(e)$ need to be very, very good indeed. Structural chemists in fact, are invariably not interested in the total energies of Eqs. (1) and (2) but in the energy differences between two systems. In the case of molecules the Mulliken–Walsh diagram is a well-established way to theoretically describe the energetic preference for

[1] Camille and Henry Dreyfus Teacher-Scholar.

0022-4596/85 $3.00

one structure over a distorted variant (or vice versa) as a function of electron count. The reasons behind the slopes of the levels on changing the geometry may be viewed from several different perspectives, and include overlap arguments and first- and second-order Jahn–Teller approaches.

In the solid state similar arguments may be used. For example, the energy changes involved in the geometrical distortion of the CaC_2 structure to that of pyrite (FeS_2) may be understood (*1*) in much the same way as the acetylene (C_2H_2) to hydrogen peroxide (O_2H_2) distortion. In more complex systems, in order to understand the energy differences between two structures from their relevant $\rho(e)$ diagrams, projection out of partial densities of states are often useful. Then the movement up or down in energy of such partial densities on distortion may be followed in an analogous fashion to that used in molecules.

These approaches provide key ways to understand the energetics of particular systems by focusing on the orbital reasons behind the changes in $\rho(e)$ on distortion. We will describe in this article a rather different method which enables some comments to be made on such energetic behavior in much broader orbital terms.

Generation of $\rho(e)$

The best known method (*2–4*) for constructing $\rho(e)$ for a molecule or solid involves solution of the secular determinant of

$$|H_{ij} - S_{ij}E| = 0, \tag{3}$$

where the H_{ij} are the Coulomb ($i = j$) and resonance ($i \neq j$) integrals linking the basis obitals of the molecule or unit cell. For the molecular case the basis set may be the valence orbitals of the molecule $\{\phi_i\}$, for the solid the basis orbitals are the Bloch sums $\{\phi_i(\mathbf{k})\}$

$$\phi_i(k) = \sum_j \exp(i\mathbf{k} \cdot \mathbf{R}_j)\chi_j(\mathbf{r} - \mathbf{R}_j), \tag{4}$$

where $\mathbf{k}$ is the wavevector and χ_j the orbital contents of the unit cell. In the molecular situation, solution of Eq. (3) just once enables the generation of the energy spectrum of **1**. For the infinite solid, solution of Eq. (3) at a representative collection of $\mathbf{k}$ points (ranging perhaps from just a few to several thousand, depending on the system) enables the construction of histogram for $\rho(e)$ by counting the number of levels located within small energy increments. A little cosmetic smoothing leads to the generation of the final density of states diagram of Fig. 1. Obviously as the number of $\mathbf{k}$ points used increases, so a more accurate $\rho(e)$ is produced.

A second method, and the one we will develop in the rest of this article is based on the method of moments (*5–7*). It has been available for many years but has found relatively little favor for the generation of $\rho(e)$ curves. By its nature this article will be very much an overview of the approach we take. Details concerning the physical reasoning and mathematical background associated with the method are neglected. These may be found elsewhere (*8–10*). First we define the nth moment of the energy density of states

$$\text{discrete case} \quad \mu_n = \sum_i e_i^n \tag{5}$$

$$\text{continuous case} \quad \mu_n = \int_{-\infty}^{\infty} \rho(e)e^n de. \tag{6}$$

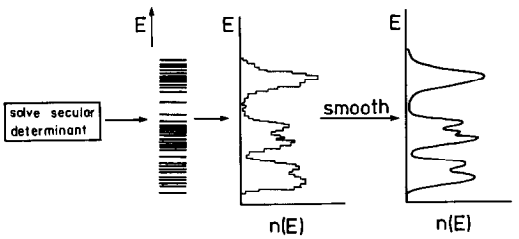

FIG. 1. Schematic showing the generation of the density of states for a solid-state system by repeated solution of the secular determinant at many different points in $\mathbf{k}$-space.

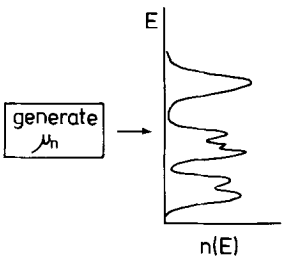

FIG. 2. Schematic showing the generation of the density of states for a solid-state system by direct inversion of a finite collection of moments. The mathematical details of the inversion process are available in Refs. (*5–9*).

With reference to Fig. 2 we will make the claim that it is possible, by knowing the moments of $\rho(e)$, to reconstruct the density of states. Figure 3 shows how, for the Hückel π levels of graphite, as the number of moments used in the reconstruction process increases, an increasingly accurate $\rho(e)$ curve is produced (*9*). This is exactly analogous to the **k**-space approach of Fig. 1, where the more points included, the more accurate the resulting $\rho(e)$ curve. Perhaps somewhat disappointing is the slow convergence of the process of Fig. 3. It is this feature which has made it an unappealing approach for the physics community, interested in details of the shape of the $\rho(e)$ curve. By contrast the one-election energy of Eq. (2) converges very rapidly indeed with increasing number of moments. For example, for graphite with a half-filled band, use of the first eight moments gives an error of 0.0007β out of total stabilization energy of 0.786β.

This is a very dramatic result because of the following. Imagine two systems which we wish to compare energetically. The brute force approach would be to proceed as in Eq. (7), via construction of

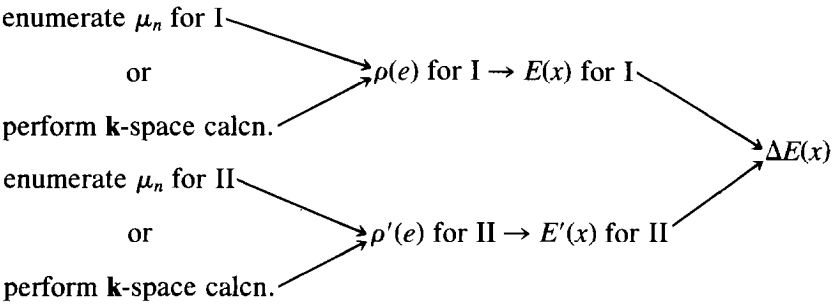

(7)

the $\rho(e)$ curves for the two structures, and evaluation of the stabilization energy of each as a function of band filling x (where empty: $0 \leq x \leq 1$: full). The $\rho(e)$ may be generated either by the **k**-space route of Fig. 1 or the moments approach of Fig. 2. However, assume that the two systems are such that their first m moments are the same. Then if $\rho(e)$ for each system is constructed using the first m moments only, the energy difference curve will be identically zero for all x. The factors influencing the energy difference between the two structures will be contained in the values of μ_n ($n > m$) and, since the stabilization energy converges rapidly with the number of moments, in the values of μ_{m+1} and to a lesser extent perhaps of μ_{m+2}. Thus a considerable improvement on the route of Eq. (7) is shown in

$$\Delta\mu_{m+1}, \Delta\mu_{m+2}, \text{ etc.} \rightarrow \Delta E(x). \tag{8}$$

The difference in the first disparate moment (and probably to a lesser extent higher moment differences) controls the energy difference curve. In other words a large

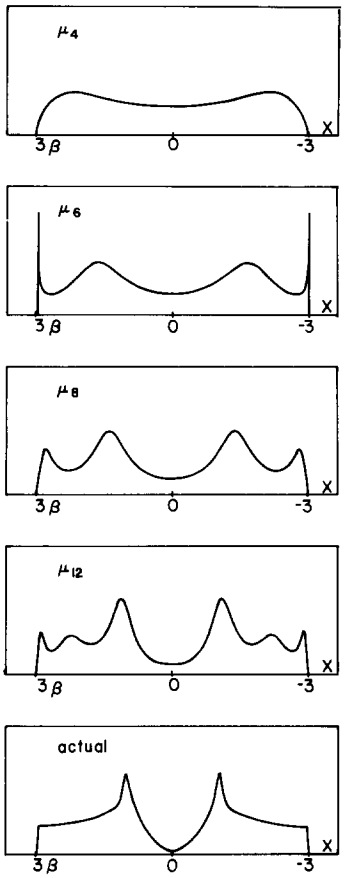

FIG. 3. Dependence of the shape of the reconstructed density of states diagram as a function of the number of moments used in the process. Notice how slowly converging the result is. (The diagram shows the result for the $p\pi$ levels of graphite.)

amount of the computational effort expended via the route of Eq. (7) in generating $\rho(e)$ and $\rho'(e)$ by either method is wasted when $\Delta E(x)$ is computed. Obviously, to profit from the route depicted in Eq. (8) we need to be able to easily calculate the moments for a given structure without recourse to the total energy density of states. We now show a very simple way of doing this.

The nth Moment

The nth moment is given by Eqs. (5) and (6) which contain the eigenvalues of the Hamiltonian. We can show that it may actually be written in a particularly simple form (5) as

$$\mu_n = \sum_{i_1,i_2,\ldots i_n} H_{i_1 i_2} H_{i_2 i_3} \cdots H_{i_n i_1}. \quad (9)$$

This equation has a simple geometrical interpretation since it may be rewritten as

$$\mu_n = \sum_{i_1} \sum_{\substack{\text{walks of} \\ \text{length } n}} H_{i_1 i_2} H_{i_2 i_3} \cdots H_{i_n i_1}, \quad (10)$$

where all walks which start at orbital ϕ_{i_1} and return in n steps are collected together. Each step from orbital j to orbital k in the walk around the lattice or molecule is weighted by the corresponding H_{jk} integral. Figure 4a shows how this perhaps surprising result is applied to the Hückel π levels of square cyclobutadiene. All walks of length 2 and of length 4 from a given orbital are enumerated. We know that (relative to $\alpha = 0$) the $p\,\pi$ levels appear as in **3**, where β

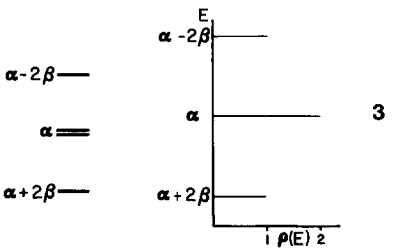

is used in its usual Hückel sense. Thus $\mu_2 = 8\beta^2$, $\mu_4 = 32\beta^4$, etc. All μ_n where n = odd are equal to zero, a direct result of the alternate or bipartite nature of the problem. For each orbital in the molecule there are but two walks of length two which return to the starting orbital, one initially moving clockwise, and the other initially moving counterclockwise. Each walk is weighted by β^2 and, since there are four equivalent orbitals per molecule, $\mu_2 = 4 \times 2 \times \beta^2 = 8\beta^2$. Similar considerations apply to the derivation of μ_4. Figure 4b shows a more economical way of counting the number of walks by using what we call propagation diagrams.

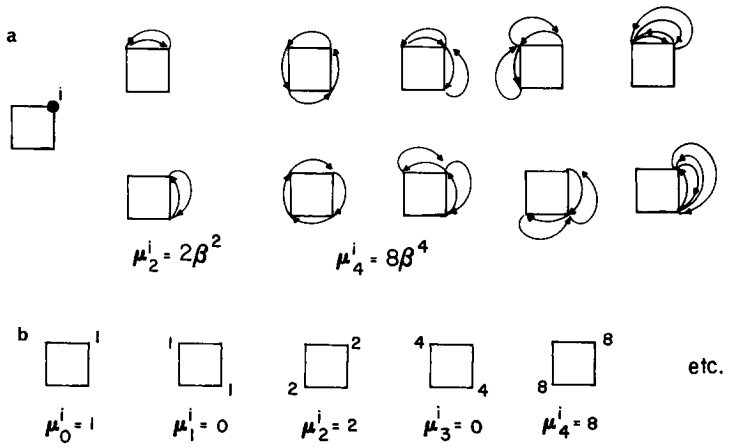

FIG. 4. Calculation of the second and fourth moments of the $p\pi$ levels of cyclobutadiene. (a) Shows the direct enumeration of the walks of length 2 and of length 4. (b) Shows a more economical way of counting the walks of given length by using a propagator which is allowed to walk around the molecule. (For simplicity we have set the Hückel α equal to zero. The scheme may be reworked without this assumption very easily.)

As we show elsewhere (*10*) for molecules with a total of m spectrum entries (**3**, for example, has three entries) we only need to know the first $2(m - 1)$ moments. Also there are ways (*11*) of determining the number of spectrum entries from the properties of the propagation diagrams. Immediately then we have not only another way to view energy level diagrams, but one which has, from Eq. (10), immediate connections with the connectivity or topology (we admit to colloquial usage of this term) of the crystal or molecular structure.

Energy Difference Curves

In the rest of this article we shall be particularly interested in understanding the energy difference curves between two structures as a function of electron count in terms of the first disparate moment of the energy density of states. We may start to tackle this problem by studying systems of the type shown in **4** and **5**. **4** is a three-tree which extends indefinitely in two dimensions. **5** contains a three-ring in the middle of this tree. Let us populate each node of these systems with a $p\pi$ orbital which lies perpendicular to the plane, and study the π density of states which results. The first disparate moment between **4** and **5** will clearly be the third, since **5** has the chance of the extra walk **6**. Similarly, a four-ring in a three-ring will differ from **4** at the fourth moment because of the extra walk, **7**, and so on. By comparison of the stabilization energy as a function of band filling of **4** relative to a system containing a m-ring in the three-tree, we may readily compute the energy difference curves $\Delta E_m(x)$. Figure 5 shows the curves for m = 2–6. Notice that they become increasingly noded as m increases, and that their ampli-

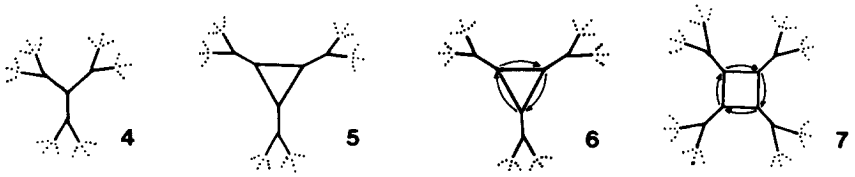

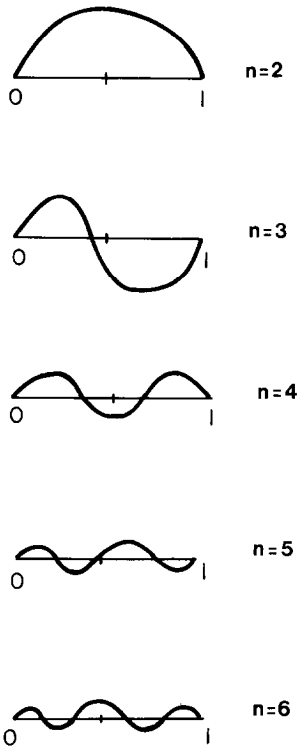

FIG. 5. $\Delta E_n(x)$ curves for n = 3–6 obtained by comparing the energy of the three-tree with that of an n-ring in a three-tree, as a function of band filling.

tude decreases. This second point is in accord with the result described earlier concerning the rapid energetic convergence with the number of moments.

For m = 3, for example, Fig. 5 tells us that the three-ring in a three-tree is more stable than the three-ring itself for band fillings which are less than a point close to the half-filled position, and less stable for higher band fillings. A similar functional form (but with different amplitudes), is found for other coordination numbers. One rather interesting observation concerning these plots is their correlation with the Hückel $4n + 2$ rule for conjugated cyclic hydrocarbons (*12*). The levels associated with the π network of C_3H_3, for example, contain three electrons. For stability in the Hückel sense, one less (n = 0) electron is needed, i.e., $C_3H_3^+$. Notice that at x = 0.5 (the situation in C_3H_3) the three-ring is destabilizing, but at x = 0.3333 (the situation in $C_3H_3^+$) the three-ring is stabilizing. Similarly the four-ring, appropriate for C_4H_4, at x = 0.5 is unstable but $C_4H_4^{+2}$ (n = 0) or $C_4H_4^{2-}$ (n = 1) correspond to values of x equal to 0.25 and 0.75, respectively, which coincide with regions of stability. The curve for the five-ring, appropriate for C_5H_5 has a node at x = 0.5, but $C_5H_5^-$ with an extra electron and corresponding to n = 1 (x = 0.625) now falls in a region of stability. The curve for the six-ring (C_6H_6) shows a stabilization at x = 0.5, the case for benzene itself (n = 1). So it appears that the Hückel rule is just a special case (for cyclic π systems) of the stabilization curves of Fig. 5.

Perhaps the most important point concerning these curves, is that although they have derived for m-rings of $p\pi$ orbitals, they represent *in general* the behavior expected for the energy difference between two arbitrary systems whose first disparate moment is the mth. Thus, although the exact shapes of the curves in the examples we describe below differ a little from those of Fig. 5, their overall shape is remarkably similar. This occurs simply because the moments associated with the σ manifold of an m-ring located in the tree will first differ from those of the three-tree itself at the mth moment. Since there are three σ-type orbitals at each center the single walk of **6** for the manifold is replaced by 3^3 σ type walks of length 3 for the three-ring. The overall effect will be the sum of these, each carrying a different weight (the product of the H_{jk}'s of Eq. (9)) because of the different orientations and overlaps of the orbitals involved. Also walks "in-place" (H_{jj}) need to be included here. Whereas we could arbitrarily set $H_{jj} = \alpha = 0$ for Hückel π levels of Fig. 4 and **3**, we cannot set to zero both s and p Coulomb integrals. Although these are added complications, the simple fact re-

mains that for an m-ring it is the mth moment which is the first to differentiate it from the simple tree. In this light it is interesting to compare the stabilization/destabilization energies of various rings relative to the simple tree, with the "ring strain" energies which organic chemists typically associate with such systems. From Fig. 5 note that three- and four-rings are both destabilized, five- (and seven) membered rings have a node in their $\Delta E_m(x)$ curves at the half-filled point, and the six-ring is stabilized. **8** compares the two approaches. The ordering in the two schemes is the same, although the reference energy zero is different in the two. Obviously not all the energy difference between the rings of varying size arises via the physical act of forming the collection of atoms into a ring. Angle changes, the traditional explanation of the organic chemist, are important too. It turns out (*9*) that for the case of the four-ring, the angle strain effect is about half as important as the effect of forming the ring itself, at the half-filled point ($x = 0.5$) which of course corresponds to the case of carbon with its four electrons per atom.

Ring size	Moment prediction	Ring strain
3,4	Strongly destabilized	Highly strained
5,7	No effect	Small strain
6	Small stabilization	Strain-free

8

Structural Stability

Perhaps the obvious place to test out these ideas is in the area of the Hückel $p\pi$ levels of plane nets. The best known example is that of graphite, the 6^3 net (**9**). With one $p\pi$ electron contributed per carbon atom, the $p\pi$ band is half-full ($x = 0.5$). **10** shows a rival structure, that of the nonmetal net in ScB_2C_2. Assuming the Sc, which lies between the layers over the seven-rings, is present as Sc(III), then the $p\pi$ band contains five electrons per four atoms, i.e., $x = 0.625$. **11** shows the energy difference curve (*9*) from a Hückel-based calculation (using the technique of Fig. 1). Satisfyingly, graphite wins out at $x = 0.5$ and ScB_2C_2 at $x = 0.625$. But how can we understand the shape of this curve? It is, in fact, quite well approximated by a linear combination of the $\Delta E_6(x)$ and $\Delta E_5(X)$ curves of Fig. 5, along with a small contribution from $\Delta E_7(x)$. Notice that $\Delta E_{5,7}(x)$ have a node at $x = 0.5$ but here $\Delta E_6(x)$ is stabilizing. Just past the half-filled point $\Delta E_6(x)$ is becoming energetically less attractive but $\Delta E_5(x)$ is becoming energetically more advantageous. By the time $x = 0.625$ the presence of five-rings in ScB_2C_2 ensures that this structure is more stable than graphite. Notice that this result is related to that described earlier concerning the Hückel $4n + 2$ rule in molecules.

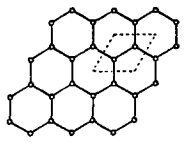

9

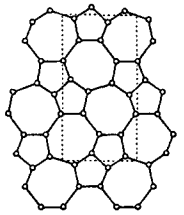

10

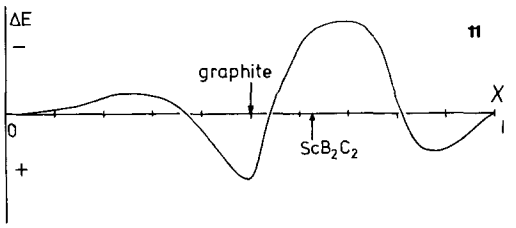

Figure 6 shows the cubic diamond structure and the hypothetical structure of "tetrahedral" diamond, derived by locating carbon tetrahedra at each of the nodes of the diamond lattice. Figure 7 shows (*9*) the calculated energy difference curve between the two structures (using the method of Fig. 1) as a function of band filling. Notice that this curve bears a striking resemblance to the $\Delta E_3(x)$ curve of Fig. 5. Indeed it should, since the cubic diamond structure contains

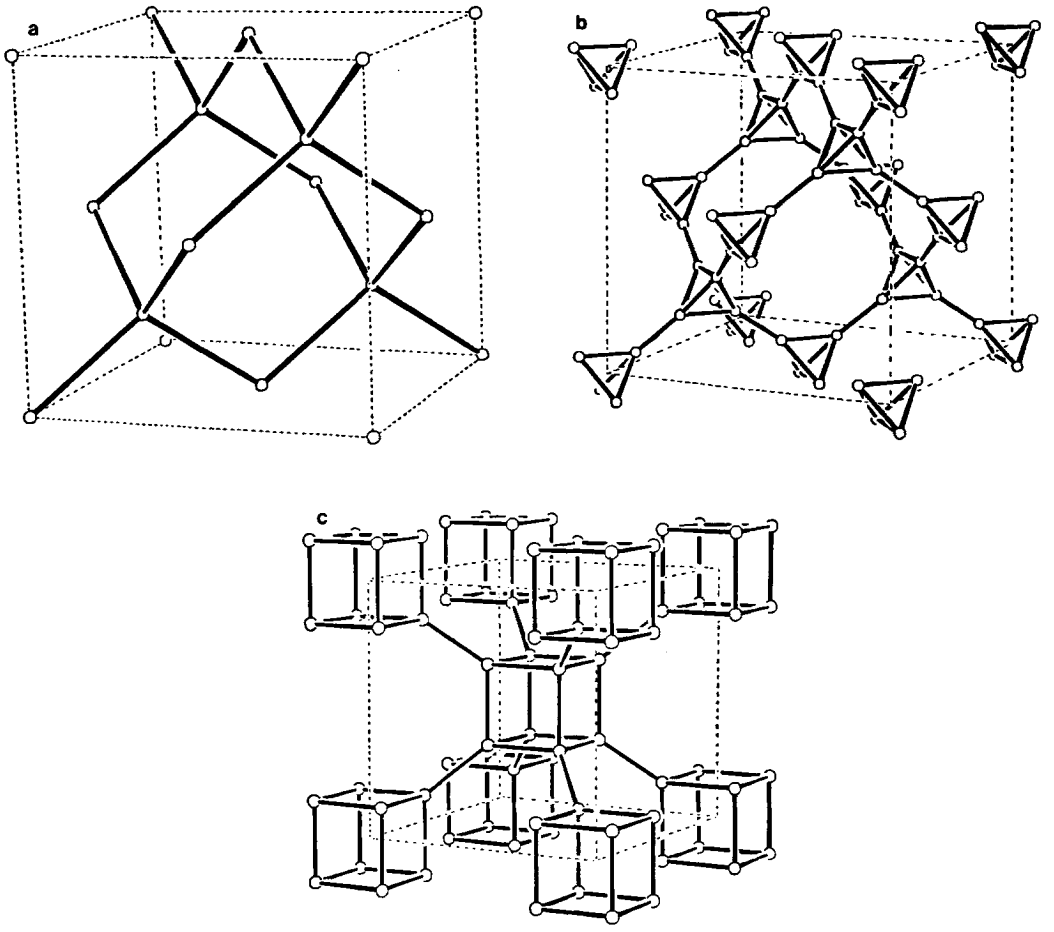

FIG. 6. The structure of (a) cubic diamond (b) "tetrahedral" diamond, and (c) "supercubane." Structures (b) and (c) are hypothetical.

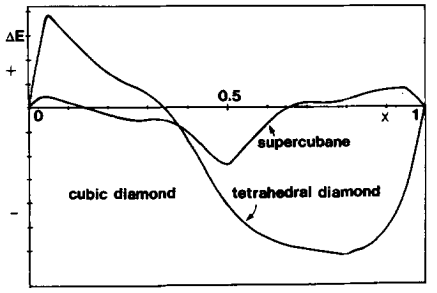

FIG. 7. Calculated energy difference curves as a function of band filling for the cubic diamond structure and the two hypothetical structures of Fig. 6, tetrahedral diamond and supercubane. When the plot is negative the cubic diamond structure is more stable.

no ring smaller than six, but the tetrahedral diamond structure is full of three-rings. Thus the first disparate moment will be the third. Satisfyingly, cubic diamond is predicted to be more stable than the alternative at the half-filled point, the electron filling corresponding to elemental carbon. Figure 6 also shows the structure of another hypothetical arrangement, supercubane. This is a body-centered lattice with cubes located at each node. This structure is dominated by the presence of four-rings. Like the other two structures in Fig. 6, this arrangement also contains four-coordinate centers.

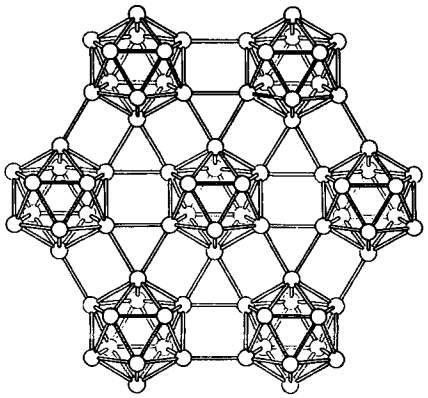

FIG. 8. The structure of rhombohedral boron. Notice the large number of three-rings.

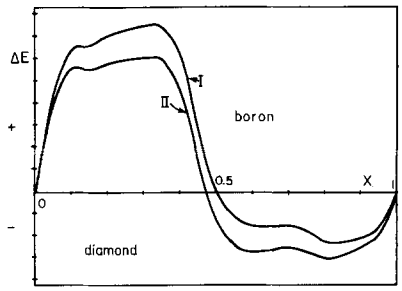

FIG. 9. Calculated energy difference curves as a function of band filling for the cubic diamond structure and the rhombohedral boron structure. The two curves represent two different geometrical models (see text). When the plot is negative the cubic diamond structure is more stable.

Figure 7 also shows the energy difference curve (*9*) between supercubane and cubic diamond. Notice that it has all the features of the curve expected for two systems whose first disparate moment is the fourth. Thus tetrahedral diamond with its three-rings and supercubane with its four-rings are destabilized at the half-filled band relative to cubic diamond with its six-rings. These two structures are predicted to be stable (relative to cubic diamond, but not perhaps with respect to some other structure) at other band fillings.

Figure 8 shows the structure of rhombohedral boron. It is a structure full of three-rings. An energy difference curve (*9*) with the cubic diamond structure is shown in Fig. 9. Two curves are shown. The one labeled I assumes equal densities for the two structures, and that labeled II assumes equal nearest neighbor distances. Both curves show the dominating influence of the $\Delta E_3(x)$ curve, but the crossing point along the x-axis is model dependent. Let us see how this comes about. To do this we need to examine the second moments of these two structures. From Eq. (9) it is obvious that the second moment is simply the sum of the squares of all the H_{ij} elements between the orbitals on an atom and its neighbors. Cubic diamond and rhombohedral diamond therefore have different second moments because of (i) the presence of six neighbors in the boron structure but only four in diamond and (ii) in model II different interatomic distances lead to different values of the H_{ij}. From Fig. 5 we expect that $\Delta E_2(x)$ will be a nodeless curve (except for those at $x = 0,1$) and that the actual energy difference curve will be (in a similar fashion to the graphite/ScB_2C_2 problem above) a mixture of $\Delta E_2(x)$ and $\Delta E_3(x)$ as shown in **12.** It is clear to see how the crossing point moves from one model to another on such a scheme.

Table I shows the crystal structures of the heavy elements at the bottom right-hand side of the Periodic Table. The structure of polonium is unusual in that it is the only known example of the simple cubic structure under ambient conditions. In this part of the Periodic Table the valence $6s^2$ pairs of electrons are often visualized as being stereochemically inert—perhaps as a

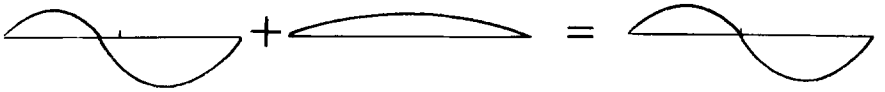

12

TABLE I

THE HEAVY ELEMENTS AT THE BOTTOM RIGHT OF THE PERIODIC TABLE

	Tl	Pb	Bi	Po
	hcp	fcc	α-Bi	Simple cubic
	s^2p^1	s^2p^2	s^2p^3	s^2p^4
$x(p$ band) =	0.167	0.333	0.5	0.677
	(assuming an inert pair)			

result of relativistic effects which make them core-like (*13*). Figure 10 shows the results of band structure calculations on the fcc, α-Bi, and simple cubic structures, which, taking advantage of this fact employ p orbitals only. Not only are the energy difference curves in good agreement with the experimental observation of the relevant structure, but the shapes of the curves look similar. In close-packed structures with high densities there will be many closed loops of length three in the structure. So the fcc and hcp structure stability will be dominated by the third moment energetics and be most stable at early band fillings (e.g., Tl, Pb). Three-rings are unfavorable at the half-filled point but six-rings are favored. Here the α-Bi structure is found with its puckered six-membered rings. The simple cubic structure is, of course, dominated by four-rings and, from Fig. 5, should be stable

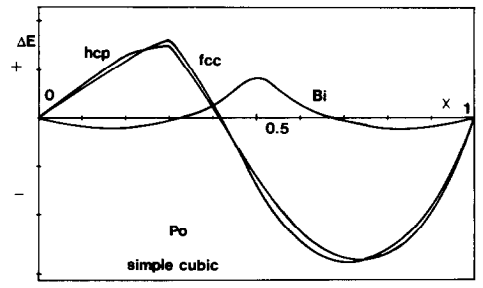

FIG. 10. Calculated energy difference curves as a function of band filling for the fcc, α-Bi, and simple cubic structures, using a p-orbital-only model. When the plot is negative the simple cubic structure is more stable.

at the three-quarters filled band. The fcc and hcp structures are obviously close in energy. The earliest moment at which they may differ is the fourth, since the structures differ at the second-nearest neighbor level only (**13**). In fact the fourth moments turn

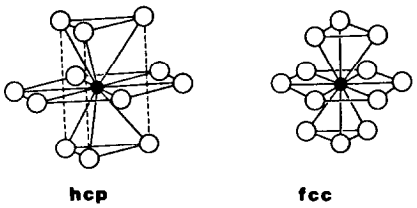

13

out (*9*) to be very similar and it is a fifth moment difference which distinguishes fcc and hcp. The hcp is stable initially (**14**) as found experimentally for thallium, and fcc is more stable later.

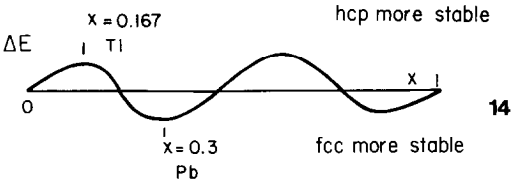

14

Stacking Problems

A problem often met in structural chemistry is that of deciding how the constituent atomic species are distributed over the sites of a lattice. A simple one-dimensional example is associated with systems of AB stoichiometry. Here A,B may be atoms or polynuclear structural units. What factors affect the relative stabilities of the . . . ABAB. . . and . . .AABB. . . arrangements? For most organic donor–acceptor complexes with other organic molecules or with coordination compounds the alternating arrangement is found, but there are some examples which contain the . . . AABB. . . pattern. In three dimensions a similar problem is encountered in the stacking of sheets of atoms. As we will see below, the . . .ABAB. . . arrangement is found for the CsCl structure but the . . .

AABB. . . for the CuTi structure, two derivatives of the bcc structure.

Our model will consider a single orbital on atoms A and B, with H_{ii} values of α_A and α_B, respectively. As an approximation we will put the resonance integral (β) equal for all AA, BB, and AB interactions. By using the walk-counting technique of Fig. 4 and including in Eq. (9) the relevant walks in place (e.g., **15, 16**) where the weight is

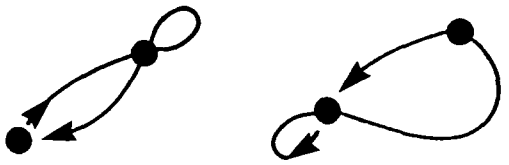

15 **16**

given by H_{ii}, it is easy to derive the first few moments of the . . .AABB. . . and . . . ABAB. . . structures (*14*). These are shown in Table II. The first disparate moment between the two structures is the fourth which is larger for the . . .AABB . . . arrangement. So the energy difference curve for the two structures as a function of band filling should look very much like $\Delta E_4(x)$ of Fig. 5. For example, at the one-quarter and three-quarters-filled band positions the . . .AABB. . . isomer should be more stable than the . . .ABAB. . . isomer, but at the half-filled point the . . . ABAB. . . structure is favored. This very simple result enables us to understand the structural differences found in organic donor–acceptor complexes (*15*). Most of these are built up from interaction between filled and empty orbitals as in **17**. There

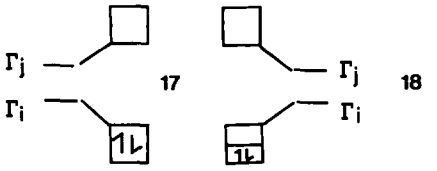

results one electron pair per two orbitals, a situation leading to $x = 0.5$. However, in NBP-TCNQF$_4$ the interaction is between a half-full orbital and an empty one (**18**) which leads to a quarter-filled band and the observation of the . . .AABB. . . arrangement (*16*). In more traditional language this particular structure can be viewed as arising via the linking of unpaired electrons to give stable A–A dimers but it requires delocalized bonding ideas to understand why this arrangement is more stable than the alternative. Figure 11 shows the calculated energy difference curve between the CsCl and CuTi structures (*17*). These are derivatives of the body-centered cubic arrangement and consist of 4^4 nets of atoms stacked up along c, each shifted $(a + b)/2$ relative to the sheet beneath it. The CsCl structure contains sheets in the . . . ABAB. . . stacking sequence, the CuTi structure, sheets in the . . .AABB. . . sequence. Notice how the energy difference curve looks very similar to the $\Delta E_4(x)$ curve of Fig. 5. (There is in fact some asymmetry due to the fact that we have set all AA, BB, and AB resonance integrals equal on our model above, whereas in practice they are different (*14*).) The dashed line in Fig. 11 shows the observed regions of stability of the two structures. Experiment and theory mesh nicely. Notice that in this example, in contrast to the linear chain problem above, there is no traditional bonding viewpoint available to view these structures.

TABLE II

MOMENTS OF STACKING ALTERNATIVES

. . .ABABAB. . .
$\mu_1 = \alpha_A + \alpha_B$
$\mu_2 = \alpha_A^2 + \alpha_B^2 + 4\beta^2$
$\mu_3 = \alpha_A^3 + \alpha_B^3 + 6\beta^2(\alpha_A + \alpha_B)$
$\mu_4 = \alpha_A^4 + \alpha_B^4 + 12\beta^2 + 6\beta^2(\alpha_A^2 + \alpha_B^2) + 8\alpha_A\alpha_B\beta^2$
. . .AABBAA. . .
$\mu_1 = \alpha_A + \alpha_B$
$\mu_2 = \alpha_A^2 + \alpha_B^2 + 4\beta^2$
$\mu_3 = \alpha_A^3 + \alpha_B^3 + 6\beta^2(\alpha_A + \alpha_B)$
$\mu_4 = \alpha_A^4 + \alpha_B^4 + 12\beta^2 + 8\beta^2(\alpha_A^2 + \alpha_B^2) + 4\alpha_A\alpha_B\beta^2$
(Assuming the only difference between A,B is a different α value)

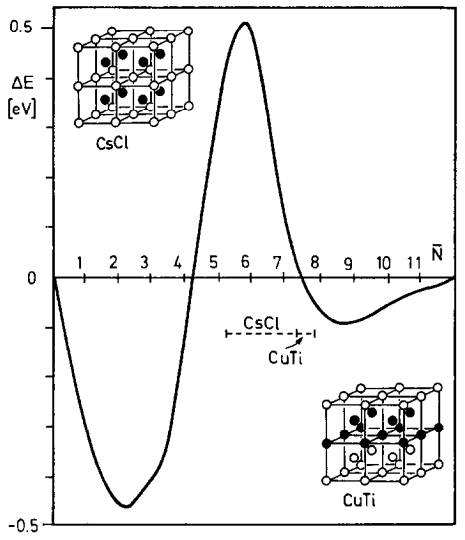

FIG. 11. Calculated energy difference curve as a function of band filling for the CsCl and CuTi structures adopted by some transition metal–transition metal alloys. The dashed line corresponds to regions where examples of these structures are found in practice.

In this section we have therefore shown that it is not always necessary to look for moment differences in terms of a loop in the form of a geometrical circuit, in order to use the $\Delta E_n(x)$ curves of Fig. 5. In the next section we show another example.

Molecules

The moments' approach may be used in the molecular area too, although it is not yet clear that the $\Delta E_n(x)$ curves of Fig. 5 will be as applicable. Figure 12 shows a comparison of some energy difference curves for the Hückel $p\pi$ levels of some two-dimensional nets with those for some 10-atomic molecules with the same ring type. Many features of the two sets of curves are similar, including the stability of the 5/7-ring structures just after the half-filled point, and the strong destabilization of the 4/8-ring structure relative to the other possibilities at the half-filled point.

Energetically the most dominant of the curves of Fig. 5 is the one corresponding to $\Delta E_3(x)$. For less than an approximately half-full band three-rings are stable, but at the half-filled point and beyond they are unfavorable structural features. It is therefore interesting to note that the structures of the (so-called "electron deficient") carboranes, transition metal carbonyl, or cy-

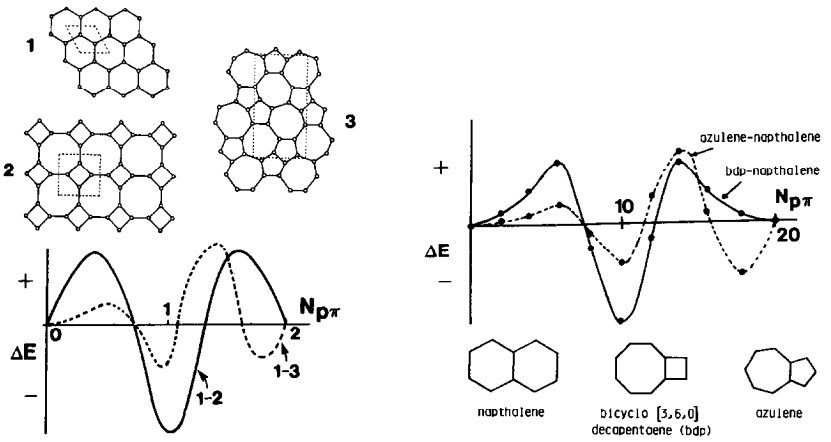

FIG. 12. Calculated energy difference curve as a function of band filling or number of electrons per molecule, for a series of two-dimensional nets and small conjugated hydrocarbons. These calculations employed the Hückel method for the out-of-plane $p\pi$ levels of these two systems.

clopentadienyl cluster compounds and the hybrid metallocarboranes are based on deltahedral frameworks. In such polyhedra every face is triangular. According to Wade's rules (*18*), the close n-vertex deltahedron is stable for a total of $(n + 1)$ skeletal electron pairs. Since there are a total of $3n$ orbitals which may be involved in skeletal bonding, this corresponds to $x = 0.3$, i.e., close to the maximum in $\Delta E_e(x)$. Notice that for the series of molecules **19**,

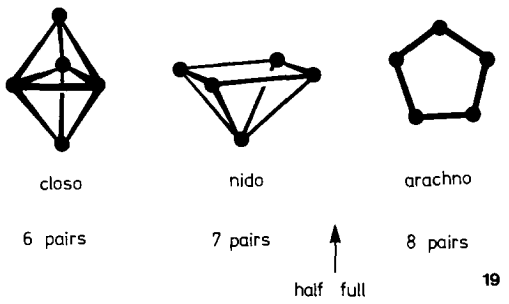

19

with the structures predicted by Wade's rules, as the electron count increases, the proportion of three-rings decreases. Eventually, for the arachno pentagonal bipyramid the "band" is more than half-full (8 skeletal pairs, 5 atoms, and 15 skeletal orbitals) the structure contains no three-rings but a single five-ring, stable just after the half-filled point.

20 shows another set of molecules

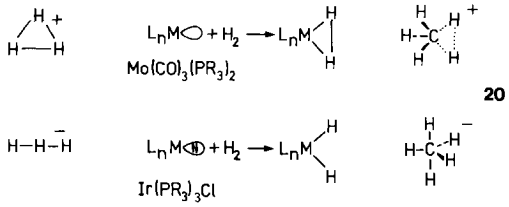

20

which show the stability of the three-ring for the case of two electrons per three orbitals ($x = 0.333$) and destruction of the three-ring for the four-electron case ($x = 0.667$). H_3^- and CH_5^- are unknown species and are calculated to be unbound. All of the other species are known.

Finally, we note that the first disparate moment between linear and bent triatomics is the fourth. Also it is the nonlinear geometry which has the larger fourth moment. The energy difference curve for the two structures will then look like $\Delta E_4(x)$. Figure 13 shows this curve, taken from Fig. 5, suitably labeled with the number of valence electrons and some examples of triatomic molecules. Notice how the linear/bent crossing point between 16 and 17 electrons (CO_2 and NO_2 for example) is accurately reproduced. In other words, contained in the moments' approach is the essence of Walsh's rules.

Caveats

We must emphasize at this point some of the restrictions of the method. First, it will only be applicable in a qualitative sense to those systems where one-electron orbital methods succeed in discriminating energetically between one structure and another. Its major utility here will be as an interpretive tool for numerical results. (It may well have a qualitative appeal in terms of the way we look at structures. Coordination polyhedra, close packings etc., all play

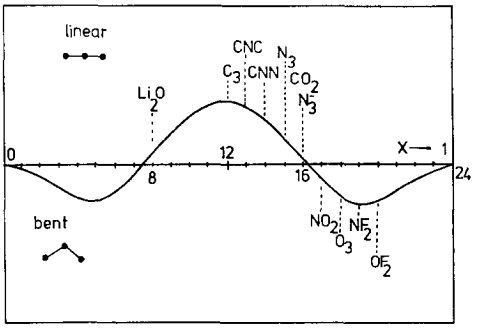

FIG. 13. The $\Delta E_4(x)$ curve from Fig. 5 labeled with the relevant electron counts for a triatomic molecule composed of main group atoms. Also shown are some representative examples.

their role in helping us organize the plethora of different structural types which have been identified. Looking at structures in terms of moments and walks provides a direct link between geometry and energetics.) One example where one-electron ideas (and hence our scheme presented here) fails is with the structure of white phosphorus and isoelectronic systems such as GeK. The three-rings which dominate the tetrahedron we claim are energetically unfavorable at this electron count. Indeed a one-electron calculation shows this structure to be much less stable than the arsenic or black phosphorus layer structures at this electron count. However, the fact remains, that although white phosphorus is not as stable as other allotropes, it does exist (as does its arsenic analog).

Second, it will have been noticed that, although the calculated energy difference curves have the same general shape as the $\Delta E_n(x)$ curves, there are many differences in detail, particularly in the crossing points. Sometimes, as in **11** and **12**, this is understandable as a result of admixture of two different $\Delta E_n(x)$ curves. Sometimes, as we discuss elsewhere (*9*) it is due to the different shapes of the $\rho(e)$ curves.

Third, the extension of the use of the $\Delta E_n(x)$ curves to molecules is not entirely straightforward. Thus the energy difference curve for the linear/bent triatomic molecular case, although containing crossings at the same places as those of Fig. 13, also contains some other structure as a result of the discrete nature of the energy level pattern. Also it will not have escaped the astute reader's attention that the crossing points for the pyramidalization of the A_4 systems do not occur where predicted using $\Delta E_4(x)$.

Acknowledgments

This research was funded by the National Science Foundation via NSF DMR 8019741 and DMR 8216892.

References

1. J. K. BURDETT AND T. J. MCLARNAN, *Inorg. Chem.* **21,** 1119 (1982).
2. (a) N. W. ASHCROFT AND N. D. MERMIN, "Solid State Physics" Saunders, Philadelphia (1976); (b) J. R. REITZ, *Solid State Phys.* **1,** 1 (1955); (c) W. A. HARRISON, "Electronic Structure and the Properties of Solids: The Physics of the Chemical Bond," Freeman, San Francisco (1980).
3. J. K. BURDETT, *Prog. Solid State Chem.*, in press.
4. M. H. WHANGBO, R. HOFFMANN, AND R. B. WOODWARD, *Proc. Roy. Soc. London Ser. A* **366,** 23 (1978).
5. F. CYROT-LACKMANN, *J. Phys. Chem. Solids* **29,** 1235 (1968); *Surf. Sci.* **15,** 535, (1969).
6. F. DUCASTELLE AND F. CYROT-LACKMANN, *J. Phys. Chem. Solids* **31,** 1295 (1970); **32** 285 (1971).
7. J. P. GASPARD AND F. CYROT-LACKMANN, *J. Phys. C.* **6,** 3077 (1975).
8. YU. V. VOROBYEV, "Methods of Moments in Applied Mathematics," Gordon & Breach, New York (1965).
9. J. K. BURDETT AND S. LEE, submitted for publication.
10. J. K. BURDETT, S. LEE, AND W. C. SHA, *Croat. Chem. Acta,* in press.
11. J. K. BURDETT, S. LEE, AND W. C. SHA, in press.
12. "Molecular Orbital Theory for Organic Chemists," Wiley, New York (1961).
13. K. S. PITZER, *Acc. Chem. Res.* **12,** 271 (1979).
14. J. K. BURDETT, T. J. MCLARNAN, AND S. LEE, submitted for publication.
15. "Extended Linear Chain Compounds" (J. S. Miller, Ed.), Plenum, New York (1982–83).
16. R. M. METZGER, N. E. HEIMER, D. GUNDEL, H. SIXL, R. H. HARMS, H. J. KELLER, D. NOTHE, AND D. WEHE, *J. Chem. Phys.* **77,** 6203 (1982).
17. J. K. BURDETT AND T. J. MCLARNAN, *J. Solid State Chem.* **53,** 382 (1984).
18. K. WADE, *Adv. Inorg. Chem. Radiochem.* **18,** 1 (1976).